Study of the $K^{\pm}\to\pi^{\pm}\pi^{0}e^{+}e^{-}$ decay by the NA48/2 experiment at CERN

2017 J. Phys.: Conf. Ser. 800 012029

(http://iopscience.iop.org/1742-6596/800/1/012029)

IOP Conf. Series: Journal of Physics: Conf. Series **800** (2017) 012029 doi:10.1088/1742-6596/800/1/012029

Study of the $K^{\pm} \to \pi^{\pm}\pi^0 e^+ e^-$ decay by the NA48/2 experiment at CERN

B Bloch-Devaux[1,2]

[1] Dipartimento di Fisica Sperimentale del Università di Torino, Torino, Italy

E-mail: brigitte.bloch@cern.ch

Abstract. The first observation of about 5000 candidates, with a 5% background contamination, of the rare decay $K^{\pm} \to \pi^{\pm}\pi^0 e^+ e^-$is reported by the NA48/2 experiment at CERN. From the analysis of 1.7×10^{11} kaon decays collected in 2003–2004, the preliminary branching ratio in the full kinematic region is measured to be $\mathcal{B}(K^{\pm} \to \pi^{\pm}\pi^0 e^+ e^-) = (4.22 \pm 0.15) \times 10^{-6}$. The observed value is in perfect agreement with theoretical predictions based on Chiral Perturbation Theory.

1. Introduction

Kaon decays have played a major role in establishing the quark mixing flavour structure of the Standard Model. Radiative kaon decays are dominated by long-distance effects but can still bring information on short-distance physics processes when considered in a detailed Dalitz plot analysis. This is the case of the $K^{\pm} \to \pi^{\pm}\pi^0 e^+ e^-$decay, never observed so far, which proceeds through virtual photon exchange followed by internal conversion into an electron-positron pair, i.e. $K^{\pm} \to \pi^{\pm}\pi^0\gamma^* \to \pi^{\pm}\pi^0 e^+ e^-$.

The virtual γ^* can be produced by two different mechanisms: Inner Bremsstrahlung (IB), where the γ^* is emitted by one of the charged mesons in the initial or final state and Direct Emission (DE) where the γ^* is radiated off at the weak vertex of the intermediate state. Consequently, the differential decay rate consists of three terms: the dominant long-distance IB contribution (pure electric part E), the DE component (electric E and magnetic M parts),

[2] for the NA48/2 Collaboration: G. Anzivino, R. Arcidiacono, W. Baldini, S. Balev, J.R. Batley, M. Behler, S. Bifani, C. Biino, A. Bizzeti, B. Bloch-Devaux, G. Bocquet, N. Cabibbo, M. Calvetti, N. Cartiglia, A. Ceccucci, P. Cenci, C. Cerri, C. Cheshkov, J.B. Chèze, M. Clemencic, G. Collazuol, F. Costantini, A. Cotta Ramusino, D. Coward, D. Cundy, A. Dabrowski, P. Dalpiaz, C. Damiani, M. De Beer, J. Derré, H. Dibon, L. DiLella, N. Doble, K. Eppard, V. Falaleev, R. Fantechi, M. Fidecaro, L. Fiorini, M. Fiorini, T. Fonseca Martin, P.L. Frabetti, L. Gatignon, E. Gersabeck, A. Gianoli, S. Giudici, A. Gonidec, E. Goudzovski, S. Goy Lopez, M. Holder, P. Hristov, E. Iacopini, E. Imbergamo, M. Jeitler, G. Kalmus, V. Kekelidze, K. Kleinknecht, V. Kozhuharov, W. Kubischta, G. Lamanna, C. Lazzeroni, M. Lenti, L. Litov, D. Madigozhin, A. Maier, I. Mannelli, F. Marchetto, G. Marel, M. Markytan, P. Marouelli, M. Martini, L. Masetti, E. Mazzucato, A. Michetti, I. Mikulec, M. Misheva, N. Molokanova, E. Monnier, U. Moosbrugger, C. Morales Morales, D.J. Munday, A. Nappi, G. Neuhofer, A. Norton, M. Patel, M. Pepe, A. Peters, F. Petrucci, M.C. Petrucci, B. Peyaud, M. Piccini, G. Pierazzini, I. Polenkevich, Yu. Potrebenikov, M. Raggi, B. Renk, P. Rubin, G. Ruggiero, M. Savrié, M. Scarpa, M. Shieh, M.W. Slater, M. Sozzi, S. Stoynev, E. Swallow, M. Szleper, M. Valdata-Nappi, B. Vallage, M. Velasco, M. Veltri, S. Venditti, M. Wache, H. Wahl, A. Walker, R. Wanke, L. Widhalm, A. Winhart, R. Winston, M.D. Wood, S.A. Wotton, A. Zinchenko, M. Ziolkowski.

and their interference. The interference term collects the different contributions, IBE, IBM and EM. In the related $K^{\pm} \to \pi^{\pm}\pi^0\gamma$ mode the interference consists only of the IBE term[1], because the remaining interferences are P-violating, and cancel out upon angular integration. In the $K^{\pm} \to \pi^{\pm}\pi^0 e^+ e^-$mode, the IBM term is a novel interference contribution. For this reason the $K^{\pm} \to \pi^{\pm}\pi^0 e^+ e^-$ decay offers interesting short and long-distance parity-violating observables that can be studied in the 3D space that now includes the non-zero $q^2 = M_{ee}^2$ kinematic variable. There are only few theoretical publications related to the $K^{\pm} \to \pi^{\pm}\pi^0 e^+ e^-$ mode [2][3][4]. The authors of [2] were able to predict, on the basis of the NA48/2 measurement of the magnetic and electric terms in the $K^{\pm} \to \pi^{\pm}\pi^0\gamma$ decay mode [5], the branching ratio of the single components. No experimental observation has so far been reported.

2. The NA48/2 experiment

The NA48/2 experiment at the CERN SPS was specifically designed for charge asymmetry measurements in the $K^{\pm} \to 3\pi$ decay modes [6]. Large sample of charged kaon ($K^{\pm}$) decays were collected during the 2003–2004 data taking period. The experiment beam line had been designed to deliver simultaneous narrow momentum band K^+ and K^- beams originating from primary 400 GeV/c protons extracted from the CERN SPS and impinging on a beryllium target. Secondary beams with central momenta of 60 GeV/c and a momentum band of $\pm 3.8\%$ (rms) were selected and brought to a common beam axis. The beam kaons decayed in a fiducial decay volume contained in a 114 m long cylindrical evacuated tank. The momenta of charged decay products were measured in a magnetic spectrometer, housed in a tank filled with helium and placed after the decay volume. The spectrometer was composed of four drift chambers (DCH) and a dipole magnet providing in the horizontal plane a momentum kick $\Delta p = 120$ MeV/c to charged particles. The momentum resolution achieved was $\sigma_p/p = (1.02 \oplus 0.044 \cdot p)\%$ (p in GeV/c). A hodoscope (HOD) consisting of two planes of plastic scintillators segmented into vertical and horizontal strip-shaped counters followed the spectrometer. The HOD surface was logically subdivided into 16 exclusive square regions producing fast signals used to trigger the detector readout on charged track topologies. Further downstream was a liquid krypton electromagnetic calorimeter (LKr), an almost homogeneous ionization chamber with an active volume of 7 m^3 of liquid krypton, $27X_0$ deep, segmented transversally into 13248 projective $\sim 2 \times 2$ cm^2 cells and with no longitudinal segmentation. The energies of photons and electrons were measured with a resoltion $\sigma_E/E = (3.2/\sqrt{E} \oplus 9.0/E \oplus 0.42)\%$ (E in GeV). An iron/scintillator hadronic calorimeter and muon detectors were located further downstream. A dedicated two-level trigger was used to collect three track decays with a very high efficiency. A detailed description of the detector can be found in [7].

3. First observation of the $K^{\pm} \to \pi^{\pm}\pi^0 e^+ e^-$ decay

The signal mode is selected simultaneously with the normalization mode ($K^{\pm} \to \pi^{\pm}\pi^0_D, \pi^0_D \to \gamma e^+ e^-$) chosen to have a final state topology ($\pi^{\pm}\gamma e^+ e^-$) differing from the signal ($\pi^{\pm}\gamma\gamma e^+ e^-$) by only one photon while satisfying similar kinematic constraints on the reconstructed π^0 and kaon masses.

3.1. Candidate selections and background estimates

Both signal and normalization candidates are reconstructed from three charged tracks (two same-sign tracks and one opposite-charge track) forming a common vertex in the fiducial decay volume (the vertex charge is then $q_{vtx} = \pm 1$). The tracks are required to be in time within 5 ns of each other using the HOD time of the hit associated to the track and their impact point should lie within the geometrical acceptance of the drift chambers (radial distance to the beam line axis, monitored by fully reconstructed $K^{\pm} \to \pi^{\pm}\pi^+\pi^-(K_{3\pi})$ events, larger than 12 cm). The track momenta are required to be in the range (2–60) GeV/c and any track-to-track distance at

DCH1 should be larger than 2 cm to suppress photon conversions to an e^+e^- pair in the upstream material. The first level trigger requires coincidences of hits in the two HOD planes in at least two of the 16 square regions. To avoid inefficiencies of geometrical origin, configurations where the three considered tracks, extrapolated to the HOD front face from positions and directions in DCH4, have their impact points in a single quadrant are rejected. This affects 2.3% of the signal simulated events and is negligible for the normalisation events while it restores high and similar trigger efficiencies for both modes.

Isolated energy clusters without associated track in the LKr, in time within 5 ns with the vertex time (mean of the three track times) are identified as the photon candidates. The minimum photon energy required is 2 GeV. The photon four-momenta are reconstructed assuming they originate from the 3-track vertex.

In the signal selection, the two-photon invariant mass is required to be within ± 15 MeV/c^2 from the nominal PDG[8] π^0 mass. The reconstructed invariant mass of the $\pi^\pm\pi^0e^+e^-$system is required to be within $\pm$ 45 MeV/c^2 from the nominal PDG $K^\pm$ mass. In the normalization selection, the same cuts applies to the invariant mass of the γe^+e^- system (π^0_D) and to the $\pi^\pm\pi^0_D$ system, respectively. The chosen ranges are loose cuts with respect to the achieved resolution for each of the reconstructed masses, minimize the dependence on possible resolution effects and maximize both acceptances.

The total reconstructed momentum is required to be in the range (54–66) GeV/c, compatible with the beam momentum and both transverse positions, of the 3-track vertex and of the reconstructed kaon at the LKr front face (defined as the energy weighted sum of the non-deviated tracks and photon(s) positions), to be consistent with the beam position as monitored by $K_{3\pi}$ events.

Kinematic identification is used instead of standard electron-pion separation based on the E/p ratio of the energy deposited in LKr and momentum measured in the spectrometer. This choice reduces the impact of particle mis-identification and increases both acceptances. The procedure assigns an electron mass to the single track with its charge opposite to q_{vtx}. The remaining electron-pion ambiguity for the two other same-sign tracks is then solved by testing the two mass hypotheses against the full selection.

The last requirement relies on the strong correlation between the reconstructed π^0 and kaon masses. This correlation can be seen in Figure 1a (Figure 2a) for the normalization (signal) mode, respectively. When selecting events within a band defined as $|M_{\pi^0} - 0.42 \cdot M_K + 73.2| < 6$ MeV/c^2 (masses in MeV/c^2), more than 99% of the normalisation simulated events and 96.5% of the signal simulated events are kept.

Two main sources of background are contributing to the signal final state: $K^\pm \to \pi^\pm\pi^0\pi^0_D$ ($K_{3\pi D}$) when one of the photons is lost, and $K^\pm \to \pi^\pm\pi^0_D(\gamma)$ ($K_{2\pi D}$), when an extra photon combines with the Dalitz photon to mimic a $\pi^0 \to \gamma\gamma$ decay. An additional suppression of the $K_{3\pi D}$ background events is obtained by requiring the squared invariant mass of the $\pi^+\pi^0$ system to be greater than 0.12 GeV$^2/c^4$, exploiting the larger phase space available in the signal mode. To reject further $K_{2\pi D}$ background contamination, each of the two possible invariant masses $M_{ee\gamma}$ are required to be more than 7 MeV/c^2 away from the nominal mass of the neutral pion. The background processes contributing to the normalization mode are $K_{\mu 3D}(K^\pm \to \mu^\pm\nu\pi^0_D)$ and K_{e3D} ($K^\pm \to e^\pm\nu\pi^0_D$) where the π^0_D is correctly reconstructed but the muon (electron) is given a pion mass and therefore can sometimes satisfy all other selection criteria.

Samples of $16.8 \times 10^6 K_{2\pi D}$ candidates and 5076 signal candidates have been selected from a subset of a 1.7×10^{11} kaon decay exposure in 2003–2004. The background estimates from simulation amount to (15182 $\pm$ 173) $K_{\mu 3D}$ events and (10334 $\pm$ 140) K_{e3D} events in the normalisation mode, corresponding to a total background contamination of 0.15%. In the signal mode, the background estimates from simulation amount to (159 $\pm$ 8) events from $K_{3\pi D}$ and (130 $\pm$ 24) events from $K_{2\pi D}$, adding up to a background contamination of 5.7%. Reconstructed

π^0_D and $\pi^\pm\pi^0_D$ mass distributions are displayed in Figures 1b,c for the selected normalisation candidates. Reconstructed $\gamma\gamma$ and $\pi^\pm\pi^0 e^+e^-$masses are shown in Figures 2b,c for the signal candidates. Expected background and normalization (signal) simulations, normalized to the number of observed candidates, show a good agreement with the data distributions.

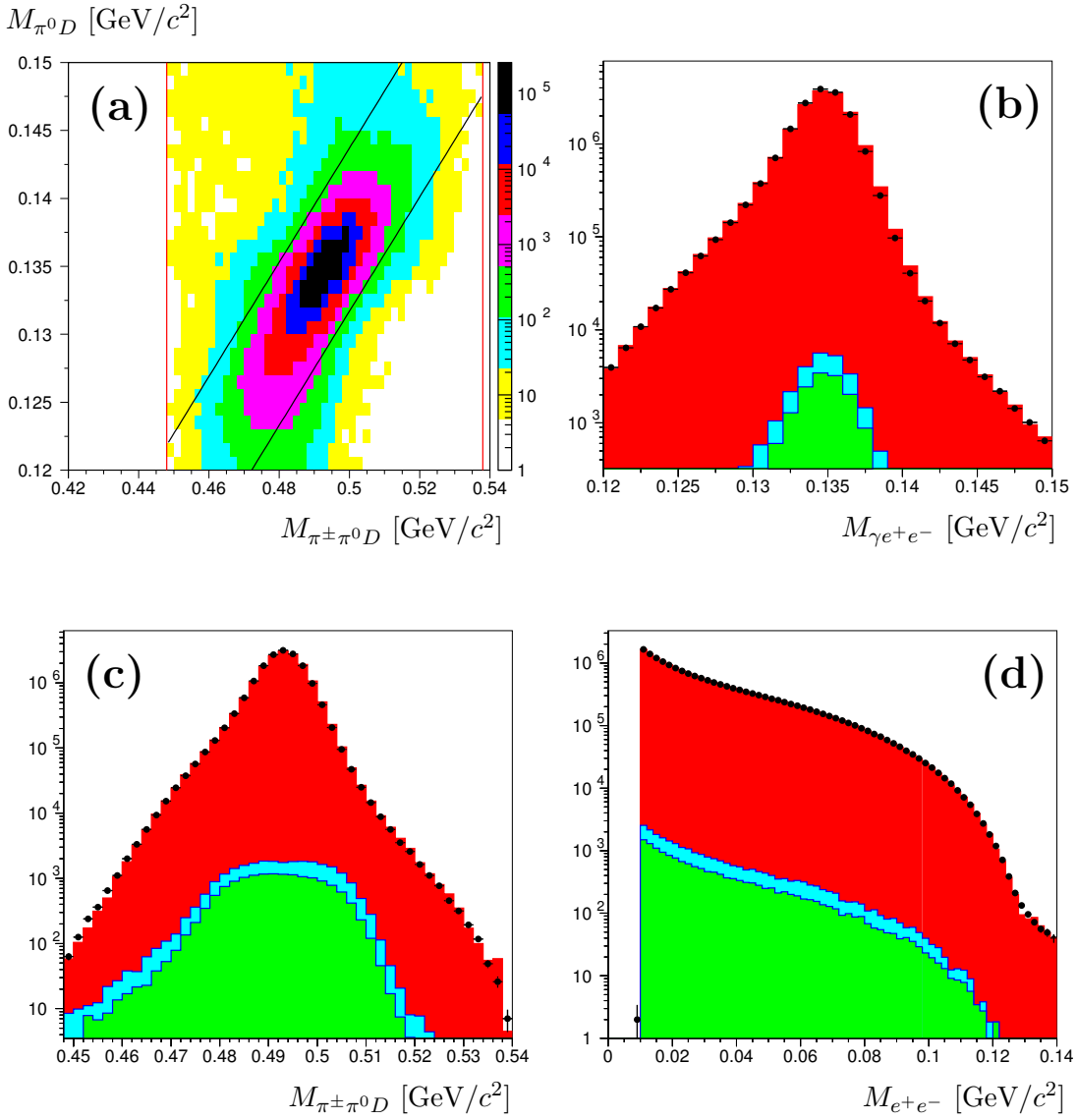

Figure 1. Normalization candidates: **(a)** Reconstructed simulated signal events in the plane $(M_{\pi^\pm\pi^0 D}, M_{\pi^0 D})$. The vertical lines shows the $M_{\pi^\pm\pi^0 D}$ selected range and the slanted band corresponds to the kinematic constraint. **(b)** Reconstructed invariant mass $M_{\pi^0 D}$ distribution. **(c)** Reconstructed invariant mass $M_{\pi^\pm\pi^0 D}$ distribution. **(d)** Reconstructed e^+e^- invariant mass distribution. The selection requires $M_{e^+e^-} > 10$ MeV/c^2 well above threshold where the acceptance is steeply falling. In the invariant mass plots, full dots correspond to data candidates, stacked histograms are, from bottom to top, the expected $K_{\mu 3D}$ and K_{e3D} backgrounds estimated from simulation and normalization best simulation including radiative effects.

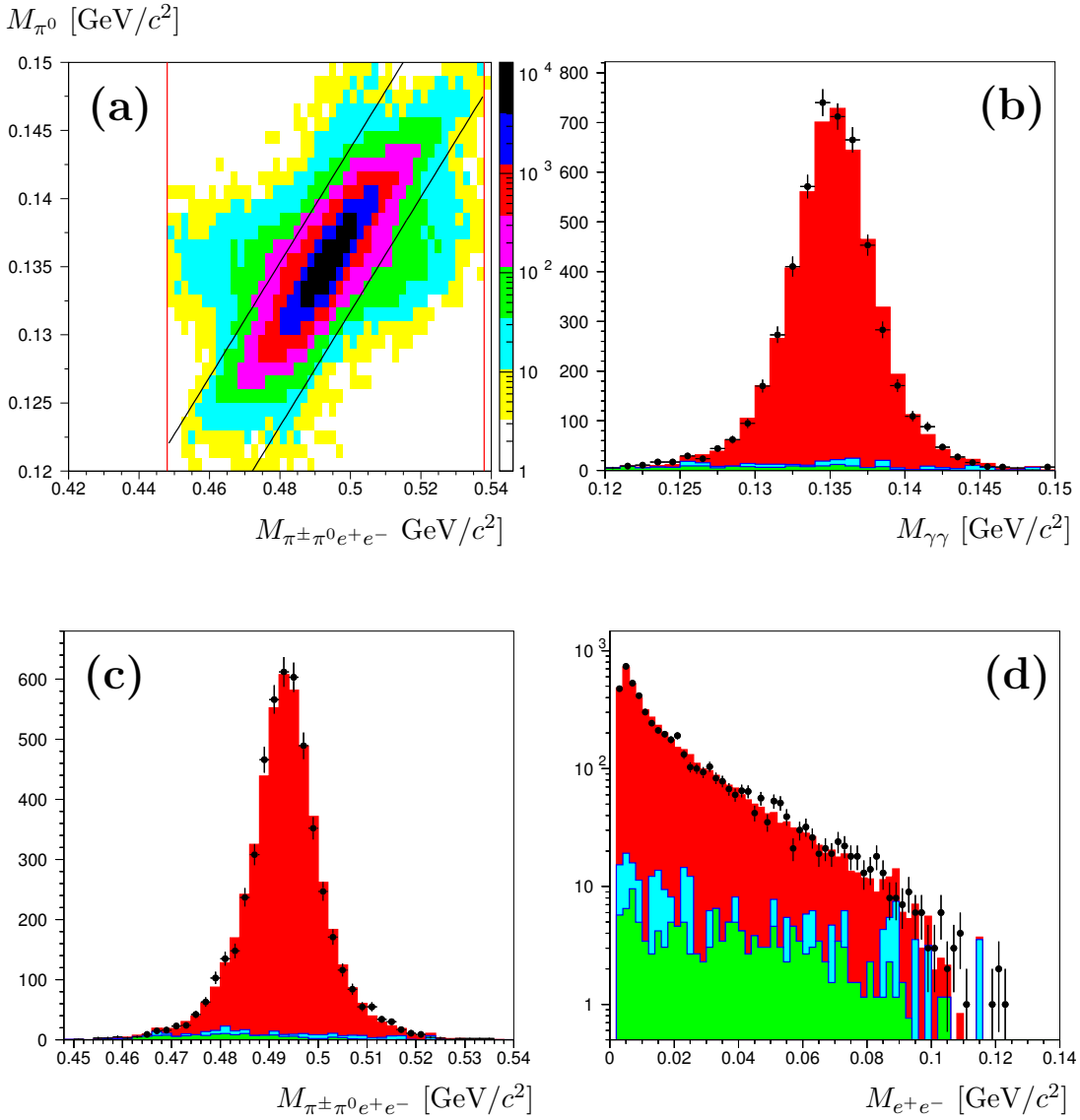

Figure 2. Signal candidates: **(a)** Reconstructed simulated signal events in the plane $(M_{\pi\pi^0e^+e^-}, M_{\pi^0})$. The vertical lines shows the $M_{\pi^\pm\pi^0e^+e^-}$ selected range and the slanted band corresponds to the kinematic constraint. **(b)** Reconstructed M_{π^0} invariant mass distribution. **(c)** Reconstructed $M_{\pi^\pm\pi^0e^+e^-}$ invariant mass distribution. **(d)** Reconstructed e^+e^- invariant mass distribution. Full dots correspond to data candidates, stacked histograms are, from bottom to top, the expected $K_{3\pi D}$ and $K_{2\pi D}$ backgrounds estimated from simulation and signal IB simulation.

3.2. Branching ratio measurement

The Branching Ratio of the $K^\pm \to \pi^\pm\pi^0e^+e^-$decay mode is obtained using the expression:

$$\mathcal{B}(K^\pm \to \pi^\pm\pi^0e^+e^-) = \frac{(N_S - N_{Bs})}{(N_N - N_{Bn})}\frac{A_N\epsilon_N}{A_S\epsilon_S}\mathcal{B}(N) \qquad (1)$$

where $N_{S,Bs,N,Bn}$ are the number of signal (5076), background to signal (289 ± 25), $K_{2\pi D}$ (16.8×10^6) and corresponding background (25517 ± 223) events. $A_{S,N}$ and $\epsilon_{S,N}$ are the

acceptances and trigger efficiencies of the signal and normalization modes. The trigger efficiency (ϵ_N), is measured using control data samples. It is also evaluated on simulated samples and found to be well reproduced ($\epsilon_N = 98.4\%$). Because of the very limited data statistics, simulated signal samples are therefore used to evaluate the signal trigger efficiency ($\epsilon_S = 99.2\%$) . The normalization mode branching ratio $\mathcal{B}(N) = (2.427 \pm 0.073) \times 10^{-3}$ is obtained from the PDG[8] world average. The acceptances of the signal, the normalization and the background channels are computed using a GEANT3-based [9] Monte Carlo (MC) simulation which includes full detector geometry and material description, stray magnetic fields, accurate beam line geometry, local detector imperfections and time variations of the above throughout the data taking period. The acceptance A_N (4.08%) is computed using the implementation of $K^\pm \to \pi^\pm\pi^0$ according to [10] followed by π^0_D according to the most recent calculations [11], including the best current implementation of radiative effects. The agreement between data and simulation can be seen from the $M_{e^+e^-}$ distribution of Figure 1d. The MC simulations for the different $\pi\pi^0e^+e^-$ contributions IB, DE, and the electric interference IBE, have been generated separately according to the theoretical description given in [2] neglecting the magnetic interference in the present preliminary result. The signal acceptance A_S (0.67%) has been obtained from a weighted average of the single component acceptances, using as weights the relative contributions with respect to IB computed in [2]:

$$A_S = \frac{A_{IB} + A_{DE} \cdot w_{DE} + A_{INT} \cdot w_{INT}}{1 + w_{DE} + w_{INT}} \tag{2}$$

To take into account the E,M measurement uncertainties in [5], the weights entering the total signal acceptance were varied accordingly resulting in a 0.25% relative change quoted as the systematic uncertainty due to the acceptance modeling. As radiative corrections to the $\pi\pi^0e^+e^-$ mode are not considered in [2], the signal MC simulation included both the classical Coulomb attraction/repulsion between charged particles and the real photon(s) emission as implemented in the PHOTOS package. The preliminary result for the total branching ratio is obtained:

$$\mathcal{B}(K^\pm \to \pi^\pm\pi^0e^+e^-) = (4.22 \pm 0.06_{stat.} \pm 0.04_{syst.} \pm 0.13_{ext.}) \times 10^{-6} \tag{3}$$

where systematic errors include uncertainties on acceptance, trigger efficiencies and radiative corrections. The external error originating from the normalisation mode branching ratio uncertainty is the dominant error in the present measurement obtained with an overall precision of about 3%.

In summary, the first experimental measurement of the branching ratio $\mathcal{B}(K^\pm \to \pi^\pm\pi^0e^+e^-)$ $= (4.22 \pm 0.15) \times 10^{-6}$ is in very good agreement with the theoretical predictions [2] of 4.19×10^{-6} without Isopsin breaking corrections and 4.10×10^{-6} including Isospin breaking corrections. The NA48/2 data sample analyzed has no sensitivity to the DE and INT contributions to the M_{ee} spectrum within the current statistics (Figure 2d). It will be difficult to perform a full Dalitz plot analysis without a proper description of the radiative effects, particularly relevant in a final state with two electron/positron.

References

[1] Christ N 1967 Phys. Rev. **159** 1292
[2] Cappiello L, Cata O, D'Ambrosio G and Gao D N 2012 Eur. Phys. J. C **72** 1872
[3] Pichl H 2001 Eur. Phys. J. C **20** 371
[4] Gevorkyan S R and Misheva M H 2014 Eur. Phys. J. C **74** 2860
[5] Batley J R *et al.* [NA48/2 Collaboration] 2010 Eur. Phys. J. C **68** 75
[6] Batley J R *et al.* [NA48/2 Collaboration] 2007 Eur. Phys. J. C **52** 875
[7] Fanti V *et al.* 2007 Nucl. Instrum. Methods A **574** 443
[8] Patrignani C *et al.* [Particle Data Group] 2016 Chin. Phys. C **40** 100001
[9] GEANT3 Detector Description and Simulation Tool 1994 CERN Program Library W5013
[10] Gatti C 2006 Eur. Phys. J. C **45** 417
[11] Husek T, Kampf K and Novotny J 2015 Phys. Rev. D **92** 054027